UNIVERSITY OF CALIFORNIA

Los Angeles

Optical Properties of Graphene from the THz to the Visible Spectral Region

A thesis submitted in partial satisfaction

of the requirements for the degree

Master of Science in Electrical Engineering

by

I-Tan Lin

2012

ABSTRACT OF THE THESIS

Optical Properties of Graphene from the THz to the Visible Spectral Region

by

I-Tan Lin

Master of Science in Electrical Engineering

University of California, Los Angeles, 2012

Professor Jia-Ming Liu, Chair

In this thesis, two models are developed to describe the optical properties of graphene from the THz to the visible spectral region. We show that the optical conductivity is mainly contributed by interband carrier transitions in the visible region and by intraband carrier scattering in the THz range. Optical properties such as refractive index and transmittance can be calculated theoretically from the model in the optical range. In the THz range, the Fermi energy and the scattering rate are two important parameters in the determination of the optical conductivity. One can use these physical quantities as fitting parameters and find their values by fitting the THz model to the experimental data. The fitted results are consistent with the data and one can predict the optical conductivity and refractive index at the frequency higher than the bandwidth of our experiments. Other physical properties such as the carrier density and the mobility can also be obtained from the fitted parameters. The resultant mobilities of monolayer graphene and bilayer graphene are consistent with the results of other groups.

The thesis of I-Tan Lin is approved.

Kang Wang

Diana Huffaker

Jia-Ming Liu, committee chair

University of California, Los Angeles

2012

Table of Content

List of Figures

List of Tables

Acknoledgement

I would like to show my deepest appreciation to my advisor, Professor Jia-ming Liu, for his help and timely guidance during my research. It would not be possible to finish this thesis without his insightful opinion and knowledge. Special thanks to Professor Kuang-Hsiung Wu and his student Shi-Kai Yao in Taiwan National Chiao Tung University for graphene sample preparation and measurement. Their data greatly helps the development of the theoretical model. My gratitude also goes to my family for their encouragement and constant support throughout my graduate study. I would also like to express my thanks to my colleagues in the Photonic Research Laboratory for their advices, and my friends, Michael Tien and Mohammed AlMulla, for proofreading my thesis.

Chapter 1
Introduction

Since Kostya Novoselov *et al*. introduced the micromechanical cleavage method that produced graphene in relatively high quality in 2004 [1-2], graphene has become a subject of intense interest in the research community. Tremendous efforts have been made on the investigation on both electronic and optical properties. Graphene is a one-atom-thick 2D system with extraordinary optical and electrical properties that can be utilized in many potential applications [3-4]. The outstanding property of graphene comes from its unique crystal structure. Graphene can be considered as two triangular sublattices with two carbon atoms per unit cell. In such a structure, the energy dispersion is linear without a band gap. The linear dispersion implies a zero effective mass and ultrafast carrier dynamics. The absence of band gap makes graphene a semi-metal, distinguishing itself from other semiconductor material. These unique properties of graphene may be utilized in future electronic and optoelectronic devices. Graphene also provides a test ground for many fundamental concepts in theoretical physics.

In this thesis, I will look into the optical property of graphene in the visible and THz spectral region in Chapters 2 and 3 respectively. The model for the visible spectral region will be

developed using time-dependent first-order perturbation theory. I will theoretically show that graphene has a broad and constant absorption range in the visible spectral region in Chapter 2. In Chapter 3, I investigate the THz property of graphene both theoretically and experimentally. The THz experiment was conducted by Shi-Kai Yao, a student of Professor Kuang-Hsiung Wu's group in Taiwan National Chiao Tung University. The basic physical properties of graphene, such as the electron density, the carrier mobility, the scattering rate and the conductivity, can be obtained by fitting the model with the experiment data. The conclusion is drawn in Chapter 4. Future research directions and possible applications of the models are also discussed at the end.

Chapter 2
Optical Properties in the Visible Spectral Region

2.1 Band Structure

The band structure of graphene can be approximated using tight-binding model considering only the nearest neighbor hopping energy (γ) [5]. As shown in Figure 1, the first Brillouin zone is a hexagon with a unit cell of two atoms. The conduction band and the valance band touch at corners of the hexagon (Figure 2), which is called the Dirac point. For an intrinsic or lightly doped graphene, the Fermi level is around the Dirac point, where charge carriers only experience a linear dispersion. This linear dispersion is called the Dirac cone since it is described by the relativistic Dirac equation. To calculate optical properties of graphene in the visible range, one can consider only the Dirac cone if the photon frequency is low compared to the resonance frequency and the Fermi energy is near the Dirac point. Since the resonance energy is about 6 eV (2γ) [6], which is larger than the photon energy in the visible range, for intrinsic graphene we can

approximate the optical properties within visible range assuming linear energy dispersion. One can anticipate the approximation will fail if the Fermi level is well above γ by electric gating or impurity doping. The assumption is also not valid if photon energies are beyond the visible range.

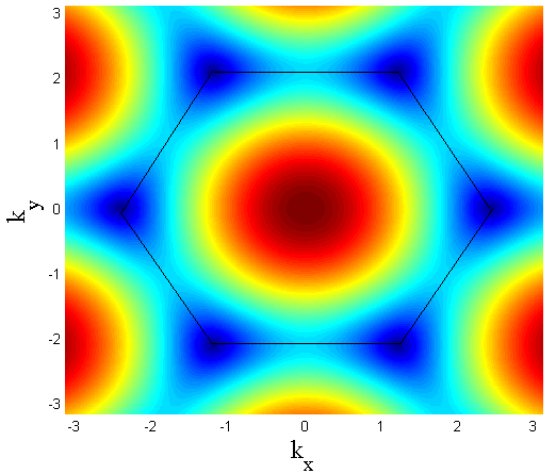

Figure 1. The first Brillouin zone of graphene. The solid line marks the boundary of the first Brillouin zone, which is in a shape of hexagon. Colors represent relative energy levels. The colormap is shown in Figure 2.

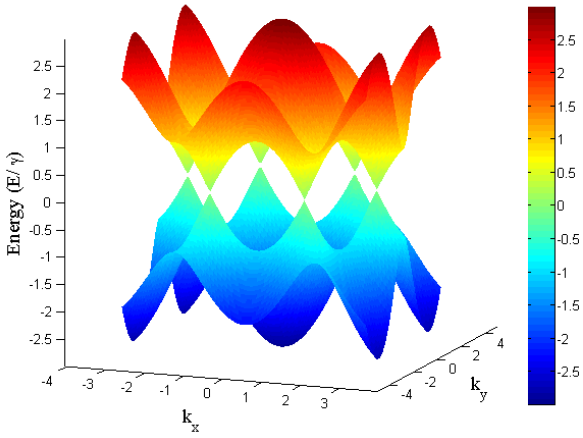

Figure 2. The band structure of graphene. The unit of energy is normalized to the nearest neighbor hopping energy γ. Six Dirac cones are shown in the vicinity of E=0 (Dirac point).

The direct result of the linear electronic dispersion of Dirac cone is effective massless fermions. The energy dispersion can be written as [7]

$$E = \pm \hbar v_f \left| \mathbf{k} \right| \tag{1}$$

where $\hbar$ is the reduced Plank's constant, v_f is the electronic group velocity or Fermi velocity, and $\mathbf{k}$ is the 2D wave vector measured from the Dirac point. The positive sign and negative sign on the right-hand side of the equation correspond to the upper part of the Dirac cone (the conduction band) and the lower part of the Dirac cone (the valance band), respectively. This

equation accounts for the electronic and optical phenomena within the visible spectral region. I will use it frequently as I develop the models for the visible and THz range.

2.2 The Model

In the visible range, photons can create electron-hole pairs by exciting electrons from the valance band to the conduction band. When the excitation happens, the photon energy is transferred to the electron. The net loss of the photon energy can be related to the imaginary part of the permittivity or the real part of the optical conductivity of graphene. Since the electrons are confined in the graphene layer, the optical conductivity is zero when the electric field is perpendicular to the graphene layer. Here we want to develop a model for the in-plane optical conductivity of graphene in the visible range. Using this model, we can also calculate the permittivity as well as the transmittance and reflectance of graphene in the visible range.

The approach I adopt here is time-dependent first-order perturbation theory using density matrix. We can first write the perturbation Hamiltonian as

$$H'(t) = -\boldsymbol{\mu} \cdot \boldsymbol{\mathcal{E}}(t), \;\; \boldsymbol{\mathcal{E}}(t) = \mathrm{Re}\left[\mathcal{E}_x e^{-i\omega t} \hat{x} \right] \tag{2}$$

where $\boldsymbol{\mu}$ is the electric dipole moment. Without loss of generality, we assume the electric field is polarized along x direction with a single frequency ω. We can ignore the momentum of photons since it is small compared with the electron crystal momentum. We can write dipole matrix elements as

$$e\left\langle c\mathbf{k}' \middle| x \middle| v\mathbf{k} \right\rangle = e\delta_{\mathbf{k}',\mathbf{k}} x_{cv} \tag{3}$$

where $\left| \; \right\rangle$ denotes eigenstates of unperturbed Hamiltonian H_o. c, v and $\mathbf{k}$ are quantum numbers

that represent the conduction band, the valance band and wave vectors respectively. Then by rotating wave approximation, we can express the perturbation Hamiltonian in the interaction picture as

$$\tilde{H}'(t) = e^{i\frac{H_o}{\hbar}t} H'(t) e^{-i\frac{H_o}{\hbar}t} = \frac{e\mathcal{E}_x}{2}\left(x_{cv} e^{i\delta t} \left|c\mathbf{k}\right\rangle\left\langle v\mathbf{k}\right| + h.c. \right) \tag{4}$$

where $\delta = (E_{c,\mathbf{k}} - E_{v,\mathbf{k}} - \hbar\omega)/\hbar$, $E_{n,\mathbf{k}}$ is eigenenergy of state $\left|n\mathbf{k}\right\rangle$, *h.c.* means Hermitian conjugate of the preceding term, and tilde sign denotes the function in the interaction picture. According to the Liouville-Von Neumann equation

$$\frac{d}{dt}\rho(t) = -\frac{\mathrm{i}}{\hbar}\left[H(t), \rho(t)\right] \tag{5}$$

where $H(t) = H_0 + H'(t)$ and $\rho(t)$ is the density matrix. It is easy to show that (5) can be translated into the interaction picture as

$$\frac{d}{dt}\tilde{\rho}(t) = -\frac{\mathrm{i}}{\hbar}\left[\tilde{H}'(t), \tilde{\rho}(t)\right] \tag{6}$$

The time evolution of the off-diagonal elements of the density matrix is

$$\begin{aligned} \frac{d}{dt}\tilde{\rho}_{cv}(t) &= \frac{d}{dt}\left\langle c\mathbf{k}\right|\tilde{\rho}(t)\left|v\mathbf{k}\right\rangle = -\frac{\mathrm{i}}{\hbar}\left[\tilde{H}_{cv}'(t)\tilde{\rho}_{vv}(t) - \tilde{\rho}_{cc}(t)\tilde{H}_{cv}'(t)\right] \\ &= -\frac{\mathrm{i}e\mathcal{E}_x}{2\hbar}\left(x_{cv}(\rho_{vv} - \rho_{cc}) e^{i\delta t} \right) \end{aligned} \tag{7}$$

Keeping in mind that it also dependents on the quantum number $\mathbf{k}$, which is eliminated from the symbol as subscript for simplicity. Integrating (7) over time, we can get

$$\tilde{\rho}_{cv}(t) = -\frac{e\mathcal{E}_x}{2\hbar}\left(\frac{x_{cv}(\rho_{vv} - \rho_{cc})}{\delta} e^{i\delta t} \right) \tag{8}$$

Now calculate electric current

$$j_{xx}(t) = -\frac{e}{A}\mathrm{Tr}[\tilde{\rho}(t)\tilde{v}_x] = -\frac{e}{A}\sum_{\mathbf{k}}\left(\tilde{\rho}_{cv}(t)\tilde{v}_{x,vc} + \tilde{\rho}_{vc}(t)\tilde{v}_{x,cv}\right) \tag{9}$$

where Tr stands for trace and A is the cross-section area. The velocity operator v_x along the x direction can be related to the position operator x by the equation of motion. For the off-diagonal element,

$$v_{x,vc} = \frac{\mathrm{i}}{\hbar}\langle v\mathbf{k}|[H,x]|c\mathbf{k}\rangle = \frac{\mathrm{i}}{\hbar}\langle v\mathbf{k}|[H_0,x]|c\mathbf{k}\rangle + \frac{\mathrm{i}}{\hbar}\langle v\mathbf{k}|[H'(t),x]|c\mathbf{k}\rangle \tag{10}$$

The second term on the right-hand side is of the order of E_x , which in turn gives (9) a quadratic term in E_x. Since we are dealing with a linear system, we shall drop it. Therefore

$$v_{x,vc} = \frac{\mathrm{i}}{\hbar}\langle v\mathbf{k}|[H_0,x]|c\mathbf{k}\rangle = \frac{\mathrm{i}x_{vc}}{\hbar}(E_{v,\mathbf{k}} - E_{c,\mathbf{k}}) = -\mathrm{i}x_{vc}\omega \tag{11}$$

$$v_{x,cv} = \mathrm{i}x_{vc}\omega \tag{12}$$

$$v_x{}^2 = v_{x,vc}v_{x,cv} = -|x|^2\,\omega^2 \tag{13}$$

where we have assumed the resonance as we did in (4); therefore, the energy difference between two levels is the photon energy as shown in (11). Translating (11) and (12) into the interaction picture and plugging them as well as (8) into (9) we have

$$j_{xx}(t) = \frac{i\omega e^2\mathcal{E}_x}{2\hbar A}\left(-e^{-i\omega t} + e^{i\omega t}\right)\sum_{\mathbf{k}}|x|^2\,\frac{\rho_{vv} - \rho_{cc}}{\delta} \tag{14}$$

since

$$\begin{aligned} j_{xx}(t) &= \mathrm{Re}[j_{xx}(\omega)e^{-i\omega t}] = \frac{1}{2}\left(j_{xx}(\omega)e^{-i\omega t} + j_{xx}{}^{\dagger}(\omega)e^{i\omega t}\right) \\ j_{xx}(\omega) &= \sigma(\omega)E(\omega) \end{aligned} \tag{15}$$

Utilizing (13), we have

$$\sigma(\omega) = -\frac{ie^2}{\omega A}\sum_{\mathbf{k}} v_x^{\,2}\,\frac{\rho_{vv}-\rho_{cc}}{E_{c,\mathbf{k}}-E_{v,\mathbf{k}}-\hbar(\omega+i\eta)} \tag{16}$$

Here we restore δ and we add an infinitesimal $i\eta$ in the frequency term so that the perturbation $H'(t) = \mu_x \,\mathrm{Re}[\mathcal{E}_x e^{-i(\omega+i\eta)t}]$ is turned off when the time is negative infinity. In order to obtain an analytical form of (16), we can apply the Dirac cone approximation where we assume the conductivity is only contributed by the carriers on the Dirac cone (1). The Dirac cone approximation is only valid if the Fermi energy and the photon energy is within the visible range. Beyond that, the energy dispersion is not linear and we can no longer adopt the approximation. In this case, a more sophisticated method has to be used. The result can be found in [8]. Here we are only interested in the visible range. Since graphene is isotropic in x and y directions, we can replace the average velocity $v_x^{\,2}$ with $v_f^{\,2}/2$ where v_f again is the electronic group velocity of carriers on the Dirac band. Using energy dispersion in (1), replacing summation with integration in (16)

$$\begin{aligned}
\sigma(\omega) &= \frac{e^2 v_f^{\,2}}{2\omega}\frac{g}{4\pi}\int_0^\infty 2\pi k\, dk\left(\rho_{vv}-\rho_{cc}\right)\delta(E_{c,k}-E_{v,k}-\hbar\omega) \\
&= \frac{e^2 v_f^{\,2}}{\omega}\int_0^\infty k\, dk\left(f(E_v)-f(E_c)\right)\delta(E_{c,k}-E_{v,k}-\hbar\omega) \\
&= \frac{e^2}{\hbar^2\omega}\int_0^\infty E\, dE\left(f(-E)-f(E)\right)\delta(2E-\hbar\omega) \\
&= \frac{e^2}{4\hbar}\left(f(-\frac{\hbar\omega}{2})-f(\frac{\hbar\omega}{2})\right)
\end{aligned} \tag{17}$$

where the identity $\lim_{\delta\to 0}(x-i\delta)^{-1} = \pi i\delta(x)$ has been used and we have dropped the imaginary part since it is relatively small in the visible spectral region [9]. g is the degeneracy of graphene which is 4 (spin plus valley degeneracy) and ρ is replaced by the Fermi-Dirac distribution f. If

we write the Fermi-Dirac distribution in terms of hyperbolic functions, (17) can be written in another form as

$$\sigma(\omega) = \frac{e^2}{4\hbar} \frac{\sinh\left(\frac{\hbar\omega}{2kT}\right)}{\cosh\left(\frac{E_f}{kT}\right) + \cosh\left(\frac{\hbar\omega}{2kT}\right)} \tag{18}$$

where E_f is the Fermi energy, k is the Boltzmann constant and T is the temperature. Equation (18) is the model for the optical conductivity of graphene in the visible range. One can use the Kubo formula and ignore many-body effect to obtain the same result [10-11]. According to (18), optical conductivities of different Fermi levels and temperatures are drawn in Figure 3. When the Fermi level is located at the Dirac point, the whole conduction band is empty while the valance band is full. There is always an electron-hole pair that can be excited by an incident photon with corresponding energy. The result is a broad absorption range for photon energy across the whole spectrum up to visible range, as the blue line shown in Figure 3. However, as the Fermi level increases, lower energy states in the conduction band will be filled gradually. Therefore, the possibility of the absorption of photon energies lower than the Fermi level will decrease because of the Pauli block. However, for graphene prepared by chemical vapor deposition (CVD), the initial doping or substrate-induced doping is on the order of 10^{12} cm^{-2} [12-13], which corresponds to a Fermi energy on the order of 100meV, far below the visible range. Therefore, when $\hbar\omega$ and kT are of the same order and E_f is much larger than $\hbar\omega$ and kT, the interband optical conductivity is approximately a constant $(\sigma_0 = e^2/4\hbar)$ in the visible range.

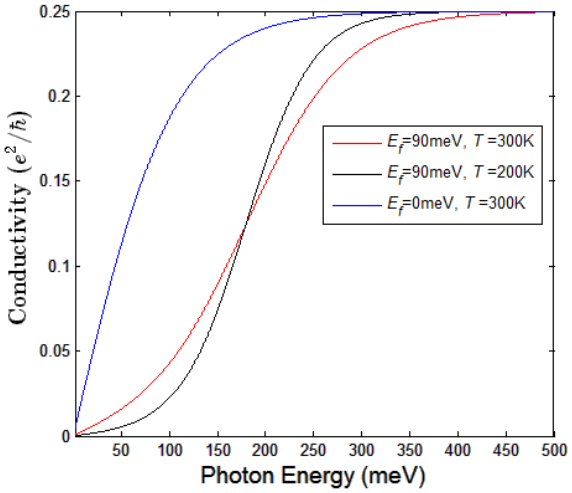

Figure 3. The optical conductivity of graphene considering only the interband carrier transition. The conductivity of different temperatures and Fermi levels are plotted together for comparison.

We can also use this constant σ_0 to estimate the permittivity of graphene in the visible range. The permittivity and the optical conductivity of graphene in the visible range is related by

$$\varepsilon(\omega) = 5.5\varepsilon_0 + i\frac{\sigma_0}{\omega d} \tag{19}$$

where ε_0 is the permittivity of vacuum and d is the thickness of graphene which is about 3.8Å [14]. $5.5\varepsilon_0$ is the background permittivity [6, 15-16]. For the wavelength of green light (546nm), the calculated relative permittivity is 5.5+5.84i, which gives the refractive index of 2.6+1.12i. The value of the refractive index of graphene is still in a debate. Different values ranging from 2+1.1i to 2.69+1.6i have been obtained from different experiments [14, 17-20]. This is due to the difficulty of simultaneously determination of the refractive index and the thickness of graphene. However, our result quantitatively matches the results from the experimental data.

The constant transmittance of 97.7% [21] can also be explained by the constant conductivity across the visible range. The transmittance of graphene in the air at normal incidence is given by

$$T = (1+\sigma_0 / 2c\varepsilon_0)^{-2} \tag{20}$$

which can be obtained straightforwardly by solving the Maxwell equation with appropriate boundary conditions. By replacing σ_0 with $e^2 / 4\hbar$ in (20), we obtain

$$T = (1+e^2 / 8\hbar c\varepsilon_0)^{-2} = (1+\pi\alpha / 2)^{-2} \cong 1-\pi\alpha \tag{21}$$

where $\alpha = e^2 / 4\pi\varepsilon_0\hbar c$ is the fine structure constant and c is the speed of light. The absorption is thus $\pi\alpha = 2.3\%$, the same as the experiment result [21].

In this chapter, I have shown that the optical conductivity of graphene in the visible range is mainly contributed by interband carrier transition. By applying the Dirac cone approximation, the optical conductivity is a constant across the visible range. One can use this constant to obtain the theoretical refractive index and transmittance in the visible range. The result quantitatively matches the results from the experiment data. However, as photon energy decrease, one cannot ignore the contribution from intraband scattering anymore. In the next chapter, I will derive a model for the optical conductivity in the THz range considering intraband carrier scattering.

Chapter 3
Optical Properties in the THz Spectral Region

3.1 Introduction

Recent terahertz technology achievements, such as THz time-domain spectroscopy and high power THz generation, have opened the door to many exciting applications in biology science, communication and sensing technology, etc [22]. Graphene is considered a promising candidate for THz detection and generation devices for many reasons. For example, the frequency of graphene plasmon and the bandgap of graphene nanoribbon are in the range of terahertz [23-24]. People have already proposed many exciting applications utilizing THz properties of graphene [4, 25-26]. In this chapter, I investigate the basic optical properties of graphene in the THz range.

3.2 The Model

Contrast to the case in the visible range, the Fermi energy is usually much larger than the photon energy in THz frequency due to the substrate-induced doping or impurity. Therefore, because of the Pauli block, the interband excitation is usually negligible in the THz case; we only have to consider the intraband interaction when building the model for the THz frequency range.

Considering constant electric field polarizing in the x direction $\boldsymbol{\mathcal{E}} = \mathcal{E}_x \hat{x}$, under the relaxation time approximation, the Boltzmann equation tells us that the carrier distribution function is

$$f(\mathbf{k}) = f^0(\mathbf{k}) - q\mathcal{E}_x v_x(\mathbf{k})\tau(\mathbf{k})\frac{\partial f^0(\mathbf{k})}{\partial E} \tag{22}$$

where $f^0(\mathbf{k})$ is the Fermi distribution function without the influence of the electric field, q is the carrier charge, $\tau(\mathbf{k})$ is the relaxation time between collisions with the impurity ions, phonons, etc., and $v_x(\mathbf{k})$ is the carrier velocity in the x direction. Using (22), the electric current can be expressed as

$$j_x = \frac{q}{A}\sum_{\mathbf{k}} f(k) v_x(\mathbf{k}) = \frac{-q^2\mathcal{E}_x}{A}\sum_{\mathbf{k}} v_x{}^2(\mathbf{k})\tau(\mathbf{k})\frac{\partial f^0(\mathbf{k})}{\partial E} \tag{23}$$

where A is the cross-section area. The summation of the first term of (22) is zero since there is no current in the absence of the electric field. Again we apply the Dirac cone approximation. The group velocity is the same across the Dirac cone. We replace $v_x{}^2(\mathbf{k})$ with $v_f{}^2/2$ as we did in (16). Noting that $\partial f^0(\mathbf{k})/\partial E$ is very small unless in the vicinity of the Fermi level, the integration is mainly contributed by wave vectors near the Fermi energy. Therefore, we can further simplify it

by putting $\tau(\mathbf{k})$ out of the integration so it represents the relaxation time near the Fermi energy. We can obtain the conductivity as

$$\sigma_{\text{mono}} = -\frac{q^2\tau}{A}\frac{{v_f}^2}{2}\sum_{\mathbf{k}}\frac{\partial f^0(\mathbf{k})}{\partial E} = -\frac{q^2\tau {v_f}^2}{2\pi^2}\int_0^\infty dk\, 2\pi k\,\frac{\partial f^0(k)}{\partial E} \tag{24}$$

where the subscript "mono" denotes the conductivity of monolayer graphene and k is $|\mathbf{k}|$ the absolute value of wave vectors. We have used the density of states of graphene in k space as $4A/(2\pi)^2$ (degeneracy of graphene is 4 [5]) . Now we want to translate it into energy space so that we can relate it to the photon energy. We can use linear dispersion relationship in (1). However, since for each value of k, there are one corresponding energy level on the conduction band and one on the valance band as shown by (1). The integration include two parts:

$$\begin{aligned}\sigma_{\text{mono}} &= -\frac{q^2\tau}{\pi\hbar^2}\left(\int_0^\infty E dE\,\frac{\partial f^0(E)}{\partial E} + \int_0^{-\infty} E dE\,\frac{\partial f^0(E)}{\partial E}\right)\\ &= -\frac{q^2\tau}{\pi\hbar^2}\int_{-\infty}^{\infty}|E|dE\,\frac{\partial f^0(E)}{\partial E}\\ &= \frac{e^2\tau}{\pi\hbar^2}2kT\ln\left(2\cosh\left(\frac{E_f}{2kT}\right)\right)\end{aligned} \tag{25}$$

where q is replaced with the electron charge -e. E_f is the Fermi energy, k is the Boltzmann constant and T is the temperature. Equation (25) is the model for the optical conductivity of graphene in the THz range. It can be reduced further if we assume $E_f \gg kT$, which is usually the case even at the room temperature. Then (25) becomes

$$\sigma_{\text{mono}} = \frac{e^2\tau}{\pi\hbar^2}E_f \tag{26}$$

In fact the relaxation time τ can be a function of temperature, impurity density or charge carrier density depending on the scattering mechanism. It is widely accepted that both short-range

scattering and long-range scattering contribute to the scattering time of monolayer graphene [27-28]. For short-range scattering, the scattering rate is proportional to E_f ; for long-range scattering, however, the scattering rate is inversely proportional to E_f . Therefore, the dependence on E_f is not linear as seen in (26) if both scattering mechanisms are present. We can also see that (26) is a real number, implying the ohmic loss due to the carrier scattering mechanism.

We can rewrite Boltzmann equation (22) in the case of oscillating field with frequency ω. The result is in the similar form of (25) but with ω dependence:

$$\sigma_{\text{mono}}(\omega) = \frac{e^2}{\pi\hbar^2}\frac{2kT}{\tau^{-1} - i\omega}\ln\left(2\cosh\left(\frac{E_f}{2kT}\right)\right) \tag{27}$$

If we set $\omega = 0$, (27) is identical to (25). Notice that in the absence of scattering $(\tau^{-1} \to 0)$, (27) is a purely imaginary number, signifying no dissipation of electric energy within graphene. However this is unlikely to happen due to the inevitable phonon scattering and finite impurity doping. Equation (27) can be further simplified as the way we did for (25) assuming $E_f \gg kT$

$$\sigma_{\text{mono}}(\omega) = \frac{e^2}{\pi\hbar^2}\frac{E_f}{\tau^{-1} - i\omega} \tag{28}$$

It is clear that (26) and (28) are just the Drude model for the graphene case.

It can be shown that for N layers of graphene, there are multiple subbands near the Dirac point [29]. For the Bernal (AB) stacking arrangement, if the number of layer N is an even number, there will be N/2 number of subbands that are parabolic with different effective masses. We call it bilayer-type subbands since the energy band is parabolic in bilayer graphene. For odd number layers, there is always one subband that is the same as the one in the monolayer graphene. We

name it monolayer-type subband. The rest (N-1)/2 subbands are bilayer-type. Therefore, the conductivity of N layers graphene is contributed by the sum of the carriers on different subbands, either monolayer-type or bilayer-type. I have shown that the optical conductivity for monolayer-type subband is that in (27). I am going to show that the conductivity contributed by bilayer-type subband is just double the value in (27). We shall ignore the interband transition between subbands since the band gaps between subbands are much larger than the photon energy in the THz range [29-30]. We will also ignore the band overlapping or band gap opening due to couplings between different lattice sites since they are small (several meV) compared to the Fermi energy [5, 29].

For a bilayer-type subband with 2D carrier density of n and effective mass m^*, the optical conductivity can be written in the form of the Drude model:

$$\sigma_{\text{bi}}(\omega) = \frac{e^2}{m^*}\frac{n}{\tau^{-1} - i\omega} \tag{29}$$

where the subscript "bi" denotes the conductivity contributed by a bilayer subband. Since both electrons on the conduction band and holes on the valance band can contribute to the conductivity, we should express the carrier density as two integrals

$$\sigma_{\text{bi}}(\omega) = \frac{e^2}{m^*}\frac{1}{\tau^{-1} - i\omega}\left(\int_0^\infty g_{\text{2D}} f(E)dE + \int_{-\infty}^0 g_{\text{2D}}\left(1 - f(E)\right)dE\right) \tag{30}$$

where $f(E)$ is the Fermi distribution and g_{2D} is the 2D density of states given by

$$g_{\text{2D}} = \frac{g_v g_s m^*}{2\pi\hbar^2} \tag{31}$$

where g_v and g_s are the valley and spin degeneracy respectively. They both have the value of 2 [5]. Plugging (31) into (30), we can obtain

$$\begin{aligned}\sigma_{\text{bi}}(\omega) &= \frac{e^2}{\pi\hbar^2}\frac{2kT}{\tau^{-1}-i\omega}\left(\ln\left(e^{E_f/kT}+1\right)+\ln\left(e^{-E_f/kT}+1\right)\right) \\ &= \frac{e^2}{\pi\hbar^2}\frac{4kT}{\tau^{-1}-i\omega}\ln\left(2\cosh\left(\frac{E_f}{2kT}\right)\right) = 2\sigma_{\text{mono}}(\omega)\end{aligned} \tag{32}$$

Therefore it shows that (29) is just double the value of (27). For N layers graphene, if N is even, the conductivity is (N/2)×2$\sigma_{\text{mono}}(\omega)$=N$\sigma_{\text{mono}}(\omega)$. If N is odd, the conductivity is still $\sigma_{\text{mono}}(\omega)$+(N-1)/2×2$\sigma_{\text{mono}}(\omega)$=N$\sigma_{\text{mono}}(\omega)$. Therefore, in the THz range, the optical conductivity is proportional to the number of layer N. It is not surprising since we have ignored the band overlapping and interband transition between subbands due to the low photon energy in the THz range. Therefore, multilayer graphene is essentially decoupled N layers graphene.

3.3 Experiment

The experiment setup and data measurement is done by Shi-Kai Yao in Taiwan at National Chiao Tung University. THz time-domain spectroscopy (THz-TDS) is used to measure the transmission of graphene in the THz range. Here I briefly explain the experiment configuration, which is similar to Ref. [31] with both pump beam and probe beam focused on graphene sample. Laser pulses are generated by mode locked Ti-sapphire laser with pulse width of 30 fs and central wavelength of 800 nm. The repetition rate is 80 MHz and the average power is about 500 mW. The laser beam is split into two beams. One is used as probe beam and another is used to pump the THz emitter (Semi-insulating InP) to generate THz pulses with a bandwidth of 0.3-2.5 THz. THz pulses are subsequently focused on the graphene sample and the transmitted signal is captured by an electro-optic THz detector (ZnTe crystal). Because of Pockels effect, the THz beam changes the refractive index of ZnTe crystal anisotropically. We can extract the transmission by measuring the intensity of the probe beam that passes through the ZnTe crystal

and polarizer beam splitter. By delaying the pump beam with respect to the probe beam, we can get the time-dependent transmission. The complex transmission data is in turn obtained by Fourier transforming the time domain data.

To better see the optical response of graphene, we first measure the transmission of the bare sapphire substrate $T_{\text{sub}}(\omega)$ without graphene sample on it. Next we measure the transmission of graphene on the substrate $T_{\text{gra}}(\omega)$ and normalize it to $T_{\text{sub}}(\omega)$

$$\frac{T_{\text{gra}}(\omega)}{T_{\text{sub}}(\omega)} = \rho(\omega)e^{i\varphi(\omega)} \tag{33}$$

where all the phase information is in the function $\varphi(\omega)$ and thus $\rho(\omega)$ is a real number. T_{gra} and T_{sub} are schematically illustrated in Figure 4. One of the major advantages of THz-TDS is the simultaneous determination and measurement of the phase and the amplitude information.

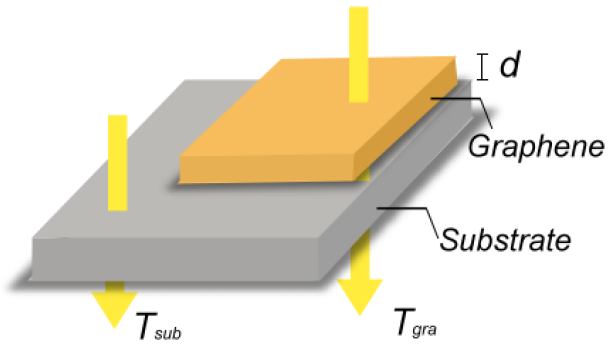

Figure 4. The schematic illustration of the THz incident light on the substrate and the graphene. *d* is the thickness of graphene. T_{gra} and T_{sub} are the transmission of graphene on the substrate and the transmission of the bare substrate respectively.

3.4 Data Analysis

By solving the Maxwell equation with suitable boundary conditions, one can show [32]

$$\frac{T_{gra}(\omega)}{T_{sub}(\omega)} = \frac{1+n}{1+n+\mathrm{N}\sigma(\omega)/c\varepsilon_0} \tag{34}$$

where n is the refractive index of the sapphire substrate, which is approximately a constant number of 3.07 within our interest THz range. We ignore its imaginary part since it is comparatively small. $\sigma(\omega)$ is the optical conductivity of monolayer graphene in (27). We drop the subscript "mono" for simplicity. c and ε_0 are the speed of light and the permittivity of vacuum respectively. N is the number of graphene layer. I have shown that the optical conductivity of N layers graphene is just N times the conductivity of monolayer graphene in the last section. Therefore, we can write $\mathrm{N}\sigma(\omega)$ as the surface conductivity of the sample with N layers. Equate (33) to (34) for the imaginary part and the real part. We can obtain two equations:

$$\sigma'(\omega) = \left(\frac{\cos(\varphi)}{\rho(\omega)} - 1\right)\frac{c\varepsilon_0(1+n)}{\mathrm{N}} \tag{35}$$

$$\sigma''(\omega) = -\frac{\sin(\varphi)(1+n)c\varepsilon_0}{\rho(\omega)\mathrm{N}} \tag{36}$$

where $\sigma'(\omega)$ and $\sigma''(\omega)$ are the real part and the imaginary part of the optical conductivity respectively ($\sigma(\omega) = \sigma'(\omega) + i\sigma''(\omega)$). Therefore, from the experimentally obtained $\theta(\omega)$ and $\rho(\omega)$, we can acquire the measured optical conductivity of the graphene sample. In the model (27), the conductivity is completely determined by two parameters, the Fermi level (E_f) and the scattering rate (τ^{-1}). For different graphene samples, the values of E_f and those of τ^{-1} will vary

because of the different imperfection and impurity densities of different samples. Take E_f and τ^{-1} as fitting parameters. By least mean square fitting of the model (27) to the experimental data (35), E_f and τ^{-1} can be extracted for any graphene sample concerned. The real part of the optical conductivity obtained from the experimental data (35) and that from the model (27) with fitted parameters, E_f and τ^{-1}, are shown in Figure 5-8 for samples of different numbers of layers. We normalized the 2D optical conductivity (Ω^{-1}) to the thickness of the sample so that it is in the unit of $\Omega^{-1}m^{-1}$. All the experiments are performed under the temperature of 294 K. The fitted results along with other calculated results are summarized in Table 1. As can be seen, with appropriate fitting numbers, the experimental data can be well described by the model.

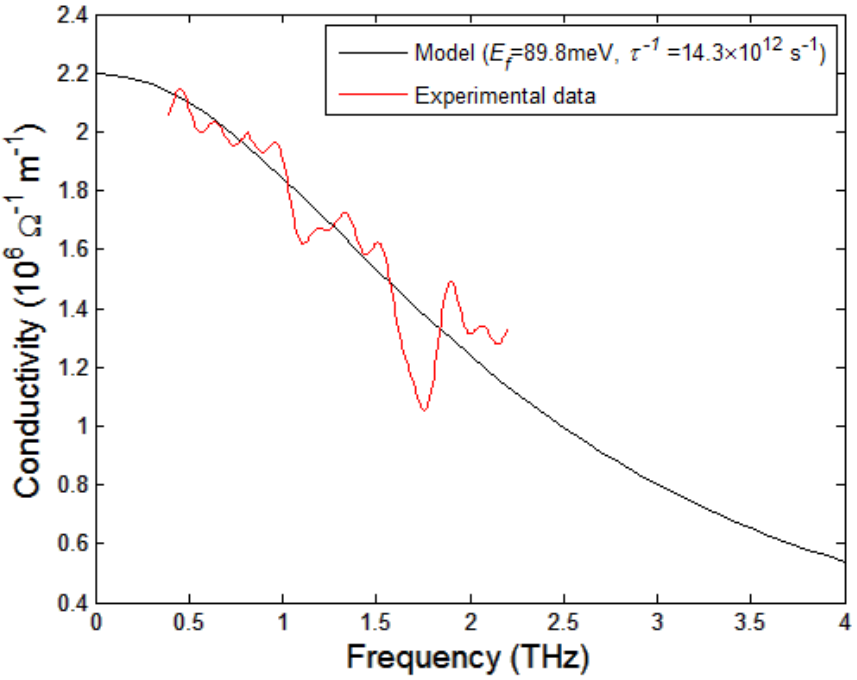

Figure 5. The measured optical conductivity and the theoretical conductivity with fitted parameters for single layer graphene. The experimental curve is best fitted with the Fermi energy (E_f) of 89.8meV and the scattering rate (τ^{-1}) of 14.3×10^{12} s^{-1}.

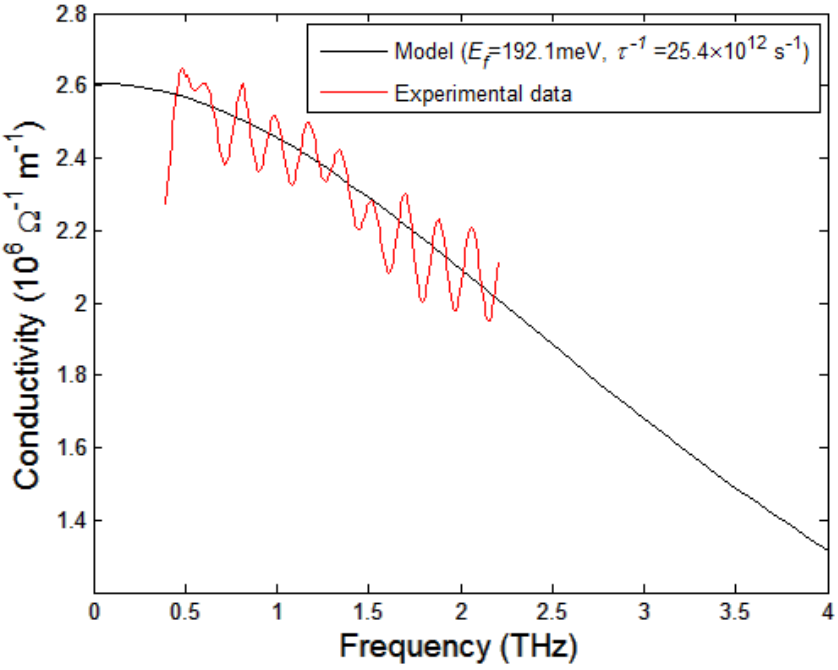

Figure 6. The measured optical conductivity and the theoretical conductivity with fitted parameters for biayer graphene. The experimental curve is best fitted with the Fermi energy (E_f) of 192.1meV and the scattering rate (τ^{-1}) of 25.4×10^{12} s^{-1}.

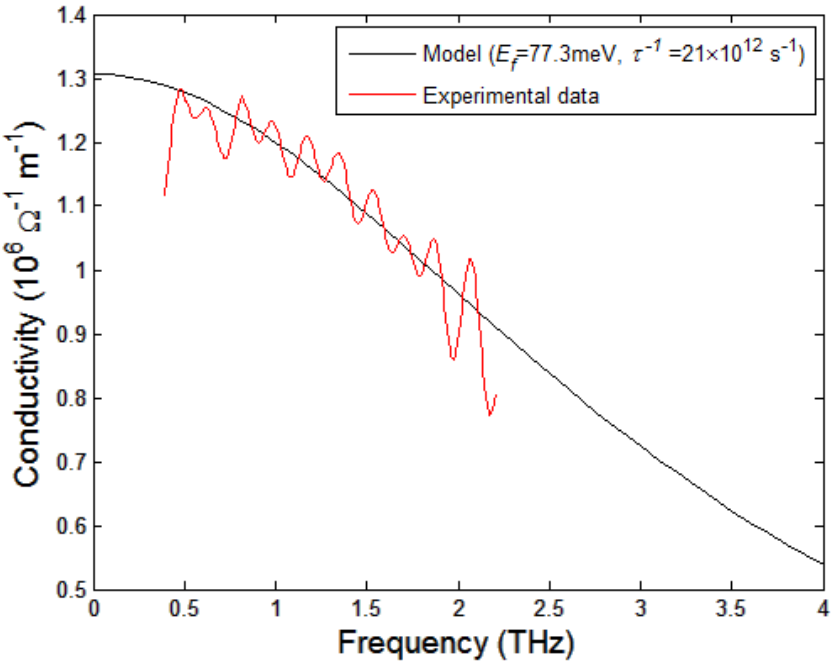

Figure 7. The measured optical conductivity and the theoretical conductivity with fitted parameters for 5 layer graphene. The experimental curve is best fitted with the Fermi energy (E_f) of 77.3meV and the scattering rate (τ^{-1}) of 21.0×10^{12} s^{-1}.

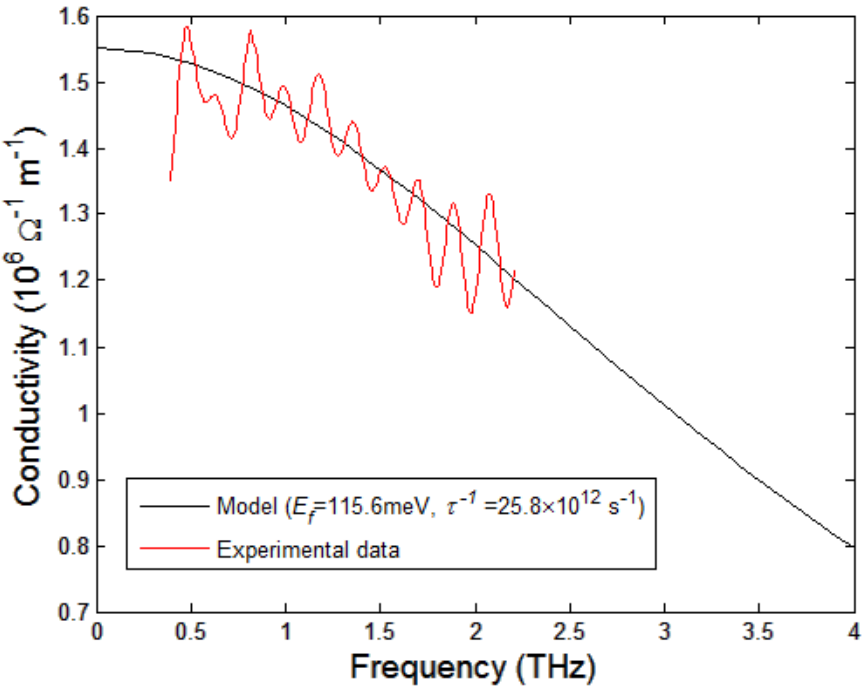

Figure 8.The measured optical conductivity and the theoretical conductivity with fitted parameters for 7 layer graphene. The experimental curve is best fitted with the Fermi energy (E_f) of 115.6meV and the scattering rate (τ^{-1}) of 25.8×10^{12} s^{-1}.

In fact, the Fermi energy can also be negative of equal fitting value and the resultant fitting curve is still the same since the optical conductivity is independent of the sign of Fermi level as shown in the model (27). To determine the sign of it, further experiment has to be done to check if it is positively doped or negatively doped. However, due to the symmetrical band structure, the mobility of electrons and holes are the same. Therefore, we don't have to know whether the majority carriers are electrons or holes in the sample to calculate the mobility. Here we assume the conductivity is contributed mostly by electrons and thus the sign of Fermi energy is chosen to be positive. With the knowledge of Fermi energy, we can now obtain the mobility of carriers by numerically calculating the density of electrons. For odd layers graphene

$$n = \int_0^\infty dE \left(\frac{2E}{\pi(\hbar v_f)^2} + g_{2D} \right) f(E) \tag{37}$$

where the first term in the brackets is the density of states of monolayer-type subband. The second term g_{2D} is the total density of states contributed by bilayer-type subbands. g_{2D} can be calculated from (31) by replacing the effective mass with the sum of different effective masses of all the bilayer-type subbands. The value of effective masses can be found in [29]. In the case of even number graphene layers, the first term in the brackets is not presented. Once we have the electron density, the electron mobility of different samples can be calculated from $\mu = \mathrm{N}\sigma(0)/ne$, where $\sigma(0)$ is given by (25) or by (27) setting $\omega = 0$. The results are shown in Table 1. As can be seen, the Fermi level is relatively high for the bilayer graphene sample. One possible explanation is that instead of AB stacking, our bilayer graphene is actually AA stacking. AA stacking bilayer is semimetal with band overlap about 0.5-0.8 eV [33-34], which gives a high conductivity even when the Fermi level is low. Investigation on AA stacking will be our future research. The mobilities calculated for monolayer graphene and bilayer graphene are similar to the results obtained in the paper [35].

Table 1. The fitted results for the Fermi level (E_f) and the scattering rate (τ^{-1}) of samples with different number of layers. The samples are assumed to be doped with electrons. 2D density of electrons (*n*) and electron mobility can be calculated from E_f and τ^{-1}.

	1 layer	2 layers	5 layers	7 layers
E_f **(meV)**	89.8	192.1	77.3	115.6
τ^{-1} **(10^{12} s^{-1})**	14.3	25.4	21.0	25.8
n **(cm^{-2})**	6.2×10^{11}	5.8×10^{12}	7.4×10^{12}	1.6×10^{13}
μ **(cm^2 V^{-1} s^{-1})**	7380	1870	1639	1360

We can relate the conductivity to the refractive index by

$$\varepsilon_r(\omega) = 2.5 + i\frac{\sigma(\omega)}{\varepsilon_0 \omega d} \tag{38}$$

$$n'(\omega) + in''(\omega) = \sqrt{\varepsilon_r(\omega)} \tag{39}$$

where $n'(\omega)$ and $n''(\omega)$ are the real part and the imaginary part of refractive index respectively. The conductivity $\sigma(\omega)$ can be obtained experimentally from (35) and (36) or theoretically from (27). Equation (38) is essentially the same as (19). The difference is that in (19) the conductivity is independent of frequency in the visible range. The resultant $n'(\omega)$ and $n''(\omega)$ are plotted in the Figure 9 and 10, respectively. As can be seen, the theoretical $n'(\omega)$ and $n''(\omega)$ with appropriate fitting numbers matches the experimental data very well. It shows that the Drude model can describe the optical conductivity of graphene up to 7 layers within our THz bandwidth.

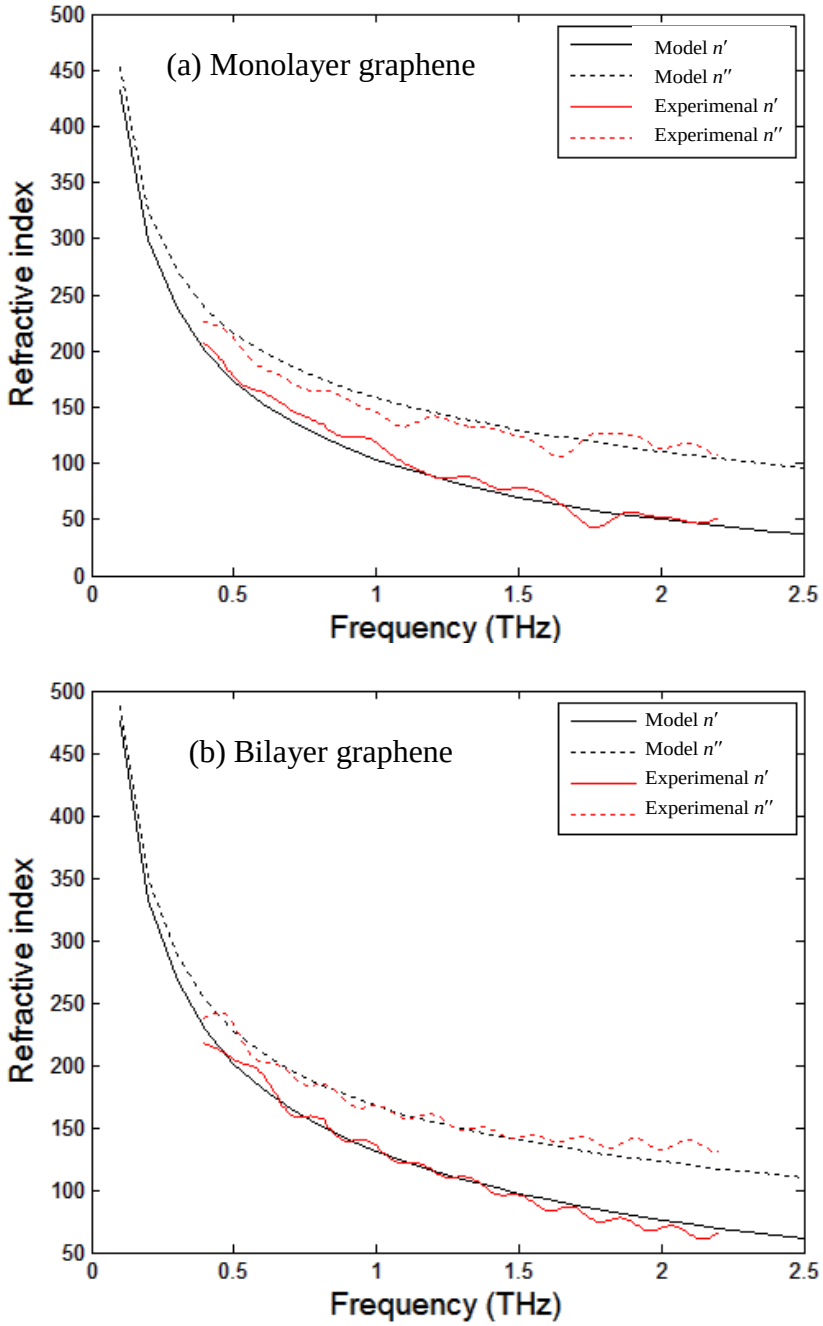

Figure 9. Refractive indexes of (a) monolayer graphene and (b) bilayer graphene. Dash lines and solid lines represent the imaginary part (k) and the real part (n) of the refractive index respectively. Red lines are calculated from the conductivity measured. Black lines are calculated from the model (27). The fitted Fermi energy and the scattering rate are 89.8meV and 14.3×10^{12} s^{-1} in (a); 192.1meV and 25.4×10^{12} s^{-1} in (b) respectively.

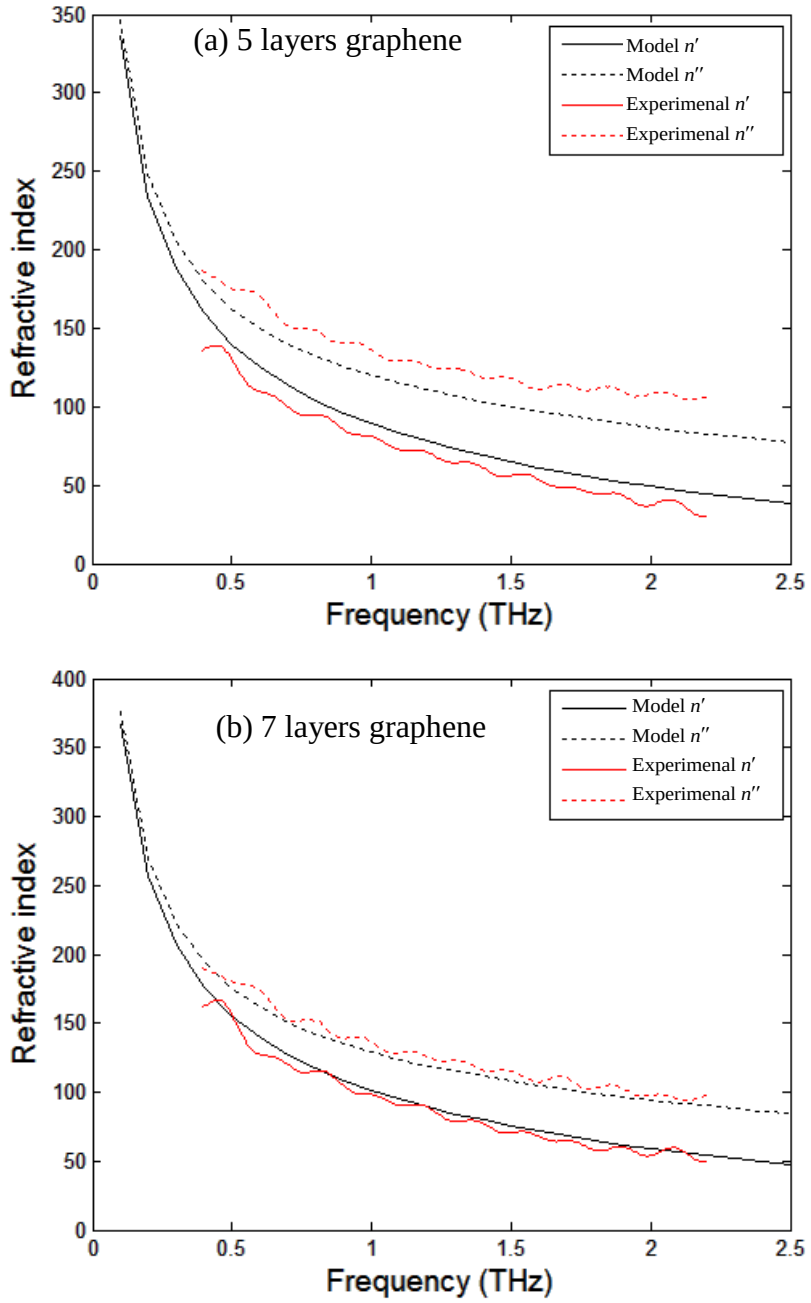

Figure 10. Refractive indexes of (a) 5 layers graphene and (b) 7 layers graphene. Dash lines and solid lines represent the imaginary part (k) and the real part (n) of the refractive index respectively. Red lines are calculated from the conductivity measured. Black lines are calculated from the model (27). The fitted Fermi energy and the scattering rate are 77.3meV and 21.0×10^{12} s^{-1} in (a); 115.6meV and 25.8×10^{12} s^{-1} in (b) respectively.

Chapter 4
Conclusion

To develop any graphene-based optoelectronic device, it is of great importance to understand the basic optical properties of graphene. I have derived models for optical conductivity in both visible and THz range. In the visible range, the optical conductivity is mainly contributed by interband carrier transitions. For the cases of intrinsic or lightly doped graphene, the optical conductivity is nearly constant, which gives a frequency independent absorption of 2.3% in the visible range. I also showed that the obtained refractive index quantitatively matches the experiment data from other groups. The optical conductivity of multilayer graphene in the THz range, in contrast, is contributed dominantly by the intraband scattering. I showed that the optical conductivity can be described by the model up to 7 layers. The Fermi energy and the scattering rate of graphene samples can be found by fitting the theoretical model to the experimental data. It showed that with appropriate fitting values, the conductivity as well as the refractive index is well described by the model. One can thus predict those physical quantities at the frequency higher than the bandwidth of the THz pulses used in the experiment.

Future work will be focused on applications of the optical conductivity models. For example, we can investigate plasmon propagation on the surface of graphene. If the optical conductivity of graphene is known, with appropriate boundary conditions, energy dispersion of plasmon can be obtained. We can also explore the possibilities of other applications such as photodetectors and optical modulators which highly rely on the understanding of the optical conductivity. Another possible direction for our future research is to derive a more comprehensive theoretical model for the optical conductivity. We can further consider the existence of finite bandgap due to symmetry breaking or many-body effects, such as electron-electron interaction and excitons.

References

1. Novoselov, K.S., et al., *Electric Field Effect in Atomically Thin Carbon Films.* Science, 2004. **306**(5696): p. 666-669.
2. Novoselov, K.S., et al., *Two-dimensional gas of massless Dirac fermions in graphene.* Nature, 2005. **438**(7065): p. 197-200.
3. Geim, A.K. and K.S. Novoselov, *The rise of graphene.* Nat Mater, 2007. **6**(3): p. 183-191.
4. Bonaccorso, F., et al., *Graphene photonics and optoelectronics.* Nat Photon, 2010. **4**(9): p. 611-622.
5. Abergel, D.S.L., et al., *Properties of graphene: a theoretical perspective.* Advances in Physics, 2010. **59**(4): p. 261-482.
6. Taft, E.A. and H.R. Philipp, *Optical Properties of Graphite.* Physical Review, 1965. **138**(1A): p. A197-A202.
7. Castro Neto, A.H., et al., *The electronic properties of graphene.* Reviews of Modern Physics, 2009. **81**(1): p. 109-162.
8. Yuan, S., H. De Raedt, and M.I. Katsnelson, *Modeling electronic structure and transport properties of graphene with resonant scattering centers.* Physical Review B, 2010. **82**(11): p. 115448.
9. Mikhailov, S.A. and K. Ziegler, *New Electromagnetic Mode in Graphene.* Physical Review Letters, 2007. **99**(1): p. 016803.
10. Gusynin, V.P., S.G. Sharapov, and J.P. Carbotte, *On the universal ac optical background in graphene.* New Journal of Physics, 2009. **11**(9): p. 095013.
11. Stauber, T., N.M.R. Peres, and A.K. Geim, *Optical conductivity of graphene in the visible region of the spectrum.* Physical Review B, 2008. **78**(8): p. 085432.
12. Horng, J., et al., *Drude conductivity of Dirac fermions in graphene.* Physical Review B, 2011. **83**(16): p. 165113.
13. Kim, J.Y., et al., *Far-infrared study of substrate-effect on large scale graphene.* Applied Physics Letters, 2011. **98**(20): p. 201907-3.
14. Gray, A., et al., *Optical detection and characterization of graphene by broadband spectrophotometry.* Journal of Applied Physics, 2008. **104**(5): p. 053109-8.
15. Klintenberg, M., et al., *Evolving properties of two-dimensional materials: from graphene to graphite.* Journal of Physics: Condensed Matter, 2009. **21**(33): p. 335502.
16. Johnson, L.G. and G. Dresselhaus, *Optical Properies of Graphite.* Physical Review B, 1973. **7**(6): p. 2275-2285.
17. Ni, Z.H., et al., *Graphene Thickness Determination Using Reflection and Contrast Spectroscopy.* Nano Letters, 2007. **7**(9): p. 2758-2763.
18. Bruna, M. and S. Borini, *Optical constants of graphene layers in the visible range.* Applied Physics Letters, 2009. **94**(3): p. 031901-3.
19. Wang, X., Y.P. Chen, and D.D. Nolte, *Strong anomalous optical dispersion of graphene: complex refractive index measured by Picometrology.* Opt. Express, 2008. **16**(26): p. 22105-22112.
20. Weber, J.W., V.E. Calado, and M.C.M. van de Sanden, *Optical constants of graphene measured by spectroscopic ellipsometry.* Applied Physics Letters, 2010. **97**(9): p. 091904-3.
21. Nair, R.R., et al., *Fine Structure Constant Defines Visual Transparency of Graphene.* Science, 2008. **320**(5881): p. 1308-1308.

22. Tonouchi, M., *Cutting-edge terahertz technology.* Nat Photon, 2007. **1**(2): p. 97-105.
23. Barone, V., O. Hod, and G.E. Scuseria, *Electronic Structure and Stability of Semiconducting Graphene Nanoribbons.* Nano Letters, 2006. **6**(12): p. 2748-2754.
24. Wang, X.F., *Plasmon spectrum of two-dimensional electron systems with Rashba spin-orbit interaction.* Physical Review B, 2005. **72**(8): p. 085317.
25. Otsuji, T., et al. (2010) *Observation of Amplified Stimulated Terahertz Emission from Optically Pumped Epitaxial Graphene Heterostructures*. ArXiv e-prints **1001**, 5075.
26. Rana, F., *Graphene Terahertz Plasmon Oscillators.* Nanotechnology, IEEE Transactions on, 2008. **7**(1): p. 91-99.
27. Stauber, T., N.M.R. Peres, and F. Guinea, *Electronic transport in graphene: A semiclassical approach including midgap states.* Physical Review B, 2007. **76**(20): p. 205423.
28. Morozov, S.V., et al., *Giant Intrinsic Carrier Mobilities in Graphene and Its Bilayer.* Physical Review Letters, 2008. **100**(1): p. 016602.
29. Koshino, M. and T. Ando, *Orbital diamagnetism in multilayer graphenes: Systematic study with the effective mass approximation.* Physical Review B, 2007. **76**(8): p. 085425.
30. Min, H. and A.H. MacDonald, *Origin of Universal Optical Conductivity and Optical Stacking Sequence Identification in Multilayer Graphene.* Physical Review Letters, 2009. **103**(6): p. 067402.
31. Ferguson, B. and X.-C. Zhang, *Materials for terahertz science and technology.* Nat Mater, 2002. **1**(1): p. 26-33.
32. George, P.A., et al., *Ultrafast Optical-Pump Terahertz-Probe Spectroscopy of the Carrier Relaxation and Recombination Dynamics in Epitaxial Graphene.* Nano Letters, 2008. **8**(12): p. 4248-4251.
33. Yuehua, X., L. Xiaowei, and D. Jinming, *Infrared and Raman spectra of AA-stacking bilayer graphene.* Nanotechnology, 2010. **21**(6): p. 065711.
34. Charlier, J.C., J.P. Michenaud, and X. Gonze, *First-principles study of the electronic properties of simple hexagonal graphite.* Physical Review B, 1992. **46**(8): p. 4531-4539.
35. Craciun, M.F., et al., *Trilayer graphene is a semimetal with a gate-tunable band overlap.* Nat Nano, 2009. **4**(6): p. 383-388.